1   **Seasonal methane accumulation and release from a gas emission site in the central North Sea**

2

3   S. Mau[1]*, T. Gentz[2], J.-H. Körber[1], M. Torres[3], M. Römer[1], H. Sahling[1], P. Wintersteller[1], R. Martinez[2],
4   M. Schlüter[2], E. Helmke[2]

5   [1] MARUM – Center for Marine Environmental Sciences and Department of Geosciences, University of
6   Bremen, Klagenfurter Str., 28359 Bremen, Germany

7   [2] Alfred Wegener Institute Helmholtz Centre for Polar and Marine Research, Am Handelshafen 12,
8   27570 Bremerhaven, Germany

9   [3] College of Oceanic and Atmospheric Sciences, Oregon State University, 104 Ocean Admin Building,
10   Corvallis, Oregon 97331-5503

11

12   * Corresponding author: Susan Mau, e-mail: smau@marum.de

13

14   Abstract
15   We investigated dissolved methane distributions along a 6 km transect crossing active seep sites at
16   40 m water depth in the central North Sea under conditions of thermal stratification in summer (July
17   2013) and homogenous water column in winter (January 2014). Dissolved methane accumulated
18   below the seasonal thermocline in summer with a median concentration of 390 nM, whereas during
19   winter, methane concentrations were typically much lower (median concentration of 22 nM). High
20   resolution methane analysis using an underwater mass-spectrometer confirmed our summer results
21   and were used to document prevailing stratification over the tidal cycle. We contrast estimates of
22   methane oxidation rates (from 0.10 to 3.99 nM day^{-1}) using the traditional approach scaled to
23   methane concentrations with microbial turnover time values, and suggest that the scaling to
24   concentration may obscure the ecosystem microbial activity when comparing systems with different
25   methane concentrations. Our measured and averaged rate constants (k') were on the order of 0.01
26   day^{-1}, equivalent to a turnover time of 100 days even when summer stratification leads to enhanced
27   methane concentrations in the bottom water. Consistent with these observations, we could not
28   detect known methanotrophs and *pmoA*-genes in water samples collected during both seasons.
29   Estimated methane fluxes indicate that horizontal transport is the dominant process dispersing the
30   methane plume. During periods of high wind speed (winter), more methane is lost to the
31   atmosphere than oxidized in the water. Microbial oxidation seems of minor importance throughout
32   the year.

33

34   1 Introduction

35   Methane is, after water vapor and CO_2, the most important greenhouse gas. Its concentration has

36   increased by a factor of 2.5 since preindustrial times, from 722 ppb in 1750 to 1800 ppb in 2011

37   (IPCC, 2013). The total global emission was estimated to be ~550 Tg (methane) yr^{-1} with an

38   anthropogenic contribution of 50 to 65%. Geological sources, which were not considered in IPCC

39   reports previously, are suggested to account for up to 30% of total emissions. These include

40   anthropogenic emissions related to leaks in the fossil fuel industry as well as natural geological seeps

41   both terrestrial and marine (IPCC, 2013). An improved emission estimate from marine seeps suggests

42   that these sources contribute ~20 Tg methane yr^{-1}, i.e., 4% of the global emissions, to the

43   atmospheric methane (Etiope et al., 2008).

44

45   In general, oceans are a minor source of methane to the atmosphere, accounting for 2-10% of the

46   global emissions (Bange et al., 1994). The main oceanic source (75%) is thought to originate from

47   estuaries, shelf and coastal areas (Bange, 2006; Bange et al., 1994). The European coastal areas were

48   found to emit 0.46-1 Tg yr^{-1}, but this value may underestimate the coastal input, since fluxes from

49   estuaries and shallow seeps have not been adequately represented (Bange, 2006).

50

51   Although continental margins account for only 10% of total ocean area and 20% of total ocean

52   primary production (Killops and Killops, 1993), more than 90% of all organic carbon burial occurs in

53   sediments deposits on deltas, continental shelves, and upper continental slopes (Berner, 1989). At

54   these locations, which are also characterized by high sedimentation rates, organic carbon is rapidly

55   buried beneath the sulfate reduction zone and becomes available to methanogens (e.g. Cicerone and

56   Oremland, 1988). Methane is also generated by thermal breakdown at high temperature and

57   pressure. A significant fraction of the methane is oxidized in anaerobic and aerobic sediments (e.g.

58   Boetius et al., 2000; Jørgensen and Kasten, 2006; King, 1992; Niewöhner et al., 1998). At cold seep

59   sites, methane escaping microbial oxidation may be transported into the overlying water either

60   dissolved in upwardly advecting pore waters or in case of oversaturation, in the form of gas bubbles.

61   Because methane is undersaturated in seawater, rising methane bubbles partially dissolve during

62   ascent through the water column (McGinnis et al., 2006), where the dissolved methane may be

63   further consumed by microbial oxidation. Only if this methane survives transport to the mixed layer,

64   it may be transferred to the atmosphere.

65

66   Because of processes consuming methane in the water column, shallow seeps are more likely to

67   contribute to the atmospheric methane pool. However, even at shallow sites, density stratification

68   may limit vertical transport. For example, at the 70 m deep Tommeliten area in the North Sea, a

69   summer thermocline constrains methane transport to the atmosphere, such that during this season

less than ~4% of the gas initially released at the seafloor reaches the mixed layer (Schneider von Deimling et al., 2011). Here we examine the seasonal cycle of methane in the North Sea by chemical and microbiological analyses of water samples collected in a region of shallow seepage during summer (July 2013) and winter (January 2014). For the case of expected seasonal stratification; we further consider whether the methane trapped in bottom waters is significantly consumed by microbial oxidation during summer, thus limiting the fraction that can be released at the onset of storm events in fall.

1.1 Study Site

The study site is situated in an area of active gas venting above a shallow gas reservoir in the central North Sea south of Dogger Bank, a sandbank that is 20 m shallower than the surrounding (Fig. 1). The gas vents are located in the Netherlands sector, license block B13 in a shallow (< 45 m) and flat region that lacks any morphological expression typical of seep structures (Schroot et al., 2005). The seeps are likely sourced from a biogenic methane reservoir (δ^{13}C values of -80‰ VPDB) of Pliocene to Pleistocene age, which lies 600-700 m below the seafloor. Patches of gas-saturated sediments between the gas reservoir and the seafloor have been imaged in seismic surveys. These data, plus observations of discreet bubble streams in the water column and rapidly decreasing methane concentrations in cores with distance from the vent site, led Schroot et al. (2005) to describe our study area as a leaking gas reservoir with laterally discontinuous seepage.

In this region, water masses from the north (Atlantic Water) and south (Straits of Dover) meet (Kröncke and Knust, 1995) and the general anticlockwise circulation along the coasts of the North Sea becomes weak and varied (Fig. 1, Howarth, 2001). Tides have the strongest influence on the currents in this region, with wind forcing becoming secondary (Howarth, 2001; Otto et al., 1990; Sündermann and Pohlmann, 2011).

Seasonal temperature stratification, common to this and other shelf seas, separates high-light and low-nutrient surface water from low-light and high-nutrient bottom water. Even though in some shelf areas, the tidal energy is sufficient to overcome stratification, Pingree and Griffiths (1978) and Holt and Umlauf (2008) have shown that our study area is situated east of the tidal front that bifurcates Dogger bank. Consequently, the water column above the Dogger sandbank is well-mixed throughout the year, whereas the deeper waters that surround the bank become stratified during spring and summer through the course of a tidal cycle.

2 Methods

105   All data used in this study was collected during two cruises with *RV Heincke*. The first cruise (HE406)

106   was conducted during summer 2013 (20.-24. July), the second cruise (HE413) during winter 2014

107   (13.-22. January).

108

109   2.1 EM710 flare imaging

110   Hydroacoustic data was collected only during the winter cruise, using a Kongsberg EM710 multibeam

111   echosounder to map active gas emissions (Fig. 2). For the precise localization of individual flares, i.e.,

112   bubble streams in an echogram, the water column data were post-processed using the Fledermaus

113   tools FMMidwater, DMagic, and the 3D Editor (© QPS). The origin of individual flares was identified

114   as the point of highest amplitudes near the seafloor. The coordinates of these points were extracted

115   using the FMGeopicker and subsequently plotted on top of the bathymetry using ArcGIS 10.2

116   (©ESRI).

117

118   For visualization of flare deflections and bubble rising heights, selected flares were extracted from

119   the water column data as point data and edited using the 3DEditor of DMagic. The processed flares

120   were plotted over the bathymetry data in a 3D-view (Fig. 2).

121

122   2.2 Water column sampling

123   To identify the size and magnitude of the dissolved methane plume generated by the bubble

124   discharge, seawater was sampled along a hydrocast transect that crossed the active gas emission

125   sites (Fig. 2). The transect extends 3 km to the east and 3 km to the west from the main bubbling

126   location denoted as cluster 1 in Fig. 2A and 2C (4°5.44'N, 55°18.36'E). To better capture the methane

127   plumes and minimize tidal current changes, the station transect was oriented in direction of tidal

128   water movement. The stations were sampled both in summer 2013 and in winter 2014; in both

129   cases, the eastern sector (5 stations) was sampled on one day (~3 h) and the western sector (5

130   stations) on another day (~3 h), so that the station directly above cluster 1 was sampled twice.

131

132   We used a rosette equipped with twelve 5 L Niskin bottles mounted on a frame that holds a Sea-Bird

133   SBE 911 plus CTD, and an SBE 43 oxygen sensor for online monitoring of salinity, temperature,

134   pressure, and dissolved oxygen. The data are archived in PANGAEA (doi:10.1594 / PANGAEA.824863

135   and doi:10.1594 / PANGAEA.832334). Twelve different water depths were sampled at each station

136   for quantification of the methane concentration and 5 water depths for methane oxidation rates.

137   Additional casts were conducted to recover sufficient water for molecular analyses.

138

139   2.2.1 Methane concentration

140   For methane concentration analysis, samples were collected in 60 ml crimp-top glass bottles, flushed

141   with 2 volumes of water and filled completely to eliminate bubbles. Bottles were immediately

142   capped with butyl rubber stoppers and crimp sealed. After adding 0.2 ml of 10 M NaOH to stop any

143   microbial activity, a 5 ml headspace of pure N_2 was introduced into each bottle as described in

144   Valentine et al. (2001) and the samples were stored at 4 °C. One to two aliquots of the headspace

145   were analyzed to determine methane concentrations using a gas-phase chromatograph equipped

146   with a flame ionization detector. The methane concentrations were calculated as detailed in Magen

147   et al. (2014). Analyses were performed both on board and post cruise. Replicate analyses of samples

148   yielded a precision of ± 5%.

149

150   2.2.2 Methane oxidation rates

151   Methane oxidation (MOx) rates were determined from ex situ incubations of water samples in 100

152   ml serum vials. Sample collection and incubation were performed as described in Mau et al. (2013).

153   Briefly, duplicate samples were collected and 50 µl of ^{3}H-labeled methane (160–210 kBq) in N_2 were

154   added to each sample. After shaking the bottles to equilibrate the tracer with the water, the samples

155   were incubated in the dark for 24 h, those collected in summer 2013 were incubated at 10 °C and

156   those from winter 2014 at 9 °C. After incubation, the total activity (^{3}H-CH$_4$ + ^{3}H-H$_2$O) in an 1 ml

157   aliquot was measured by wet scintillation counting; the activity of ^{3}H-H$_2$O was measured after

158   sparging the sample for >30 min with N_2 to remove excess ^{3}H-CH$_4$, so that the net amount of ^{3}H-CH$_4$

159   consumption can be estimated.

160

161   MOx rates were calculated assuming first-order kinetics (Reeburgh et al., 1991; Valentine et al.,

162   2001):

163

164    $MOx = k'[CH_4]$ (1)

165

166   where k' is the effective first-order rate constant calculated as the fraction of labeled methane

167   oxidized per unit time, and [CH$_4$] is the in situ methane concentration. To verify first order kinetics we

168   conducted time series incubations and measured the tracer consumption after 1, 2, 3, and 4 days.

169   The MOx values were corrected for differences between in situ and incubation temperatures

170   (Supplementary Material 1).

171

172   In addition, control samples were frequently taken and poisoned immediately after the addition of

173   the tracer. The mean ($\bar{x}$) and standard deviation (s) of all controls sampled during a cruise were

174   calculated and the limit of detection (LOD) was set as:

175

176 $$LOD = \bar{x} + 3s \tag{2}$$

177

178 The *LOD* was 0.02 nM day^{-1} and 0.09 nM day^{-1} for the summer 2013 and winter 2014 surveys,

179 respectively.

180

181 2.2.3 Analysis of bacterial communities

182 The composition of the bacterioplankton assemblages was examined using denaturing gradient gel

183 electrophoresis (DGGE) based on the 16S rRNA gene as described in Mau et al. (2013). In short,

184 immediately after sampling, 8 L of water were filtered and the bacterial cells were concentrated on

185 Nuclepore filters (0.2 µm pore size). The filters were stored on board at -20 °C and at -80 °C post

186 cruise. DNA was extracted by an UltraClean Soil DNA Kit (MoBio Laboratories, USA). 16S rRNA gene

187 specific PCR was conducted using the forward primer GM5 plus GC-clamp and the reverse primer

188 907RM (Muyzer et al., 1993) under conditions described by Gerdes et al. (2005). The PCR products

189 (ca. 500 bp) were analyzed by DGGE according to the protocol of Muyzer et al. (1993). Clearly visible

190 bands of the DGGE gels were excised from the gel. The DNA was reamplified by PCR (Gerdes et al.,

191 2005) and sequenced. The 16S rRNA gene sequences were taxonomically assigned by SILVA Online

192 Aligner (Pruesse et al., 2012).

193

194 The presence of methane-oxidizing bacteria was checked by searching for genes encoding the

195 particulate methane monooxygenase (*pmoA*), a key enzyme of methanotrophs (McDonald et al.,

196 2008). The *pmoA*-gene-specific PCR reaction was conducted by using the primer set "pmoA" and

197 amplification conditions described in McDonald and Murrell (1997).

198

199 2.3 Methane concentration analysis by underwater mass-spectrometry (UWMS)

200 In addition to the conventional methane analysis, in situ methane concentrations were quantified

201 with an UWMS during the summer 2013 cruise (Inspectr200-200, Bell et al., 2007; Gentz et al., 2013;

202 Schlüter and Gentz, 2008; Short et al., 2001; Wenner et al., 2004). The fast sampling frequency (≤ 2

203 s) of the UWMS allows mapping of methane concentrations at much higher resolution than the

204 commonly used CTD/rosette-sampling technique. The instrument consists of a membrane inlet

205 system (MIS), an Inficon (Bad Ragaz, Switzerland) Transpector CPM 200 quadruple mass

206 spectrometer, a Varian (Palo Alto, USA) turbo pump, a roughing pump, a peristaltic pump (KC

207 Denmark), an embedded PC, and a microcontroller. The UWMS was partly redesigned to include a

208 cooling system (Ricor, K508), which lowers the detection limit for methane to 16 nM. The cooling

209 system and the improvement of the detection limit are described in detail by Gentz and Schlüter

210 (2012) and Schlüter and Gentz (2008). For reproducible gas permeation through the MIS, water is

211 constantly heated to a steady temperature of 50°C and pumped at a flow rate of 3 ml min^{-1} along the

212 membrane by an external peristaltic pump.

213

214 The UWMS was deployed above the central gas seeps (cluster 1, Fig. 2) on 21.07.2013 (16:31 – 22:32

215 UTC) at five different water depths: just above the seafloor, 35 m, 28 m, 25 m, and 10 m. When the

216 system had reached the respective depth, the research vessel moved slowly along a rectangular track

217 (~125 m S-N, ~150 m E-W, Fig. 2C) surrounding the flares of cluster 1 and towed the UWMS, which

218 continuously measured the methane concentrations. Each of the 5 tows (Fig. 2C) took approximately

219 one hour and recorded 400-800 methane concentration values.

220

221 2.4 Estimation of methane fluxes

222 Advection, horizontal and vertical turbulent diffusion, sea-air flux, and microbial oxidation rates were

223 quantified for the upper (0-30 m) and lower water column (30-40 m) during summer stratification

224 (July 2013) and for the entirely mixed water column (0-40 m) in winter (January 2014).

225

226 The advective flux (*ADV*) was calculated by multiplying methane concentration (*C*) and current

227 velocity (*v*):

228

229 $ADV = vC$ (3)

230

231 Methane concentrations were averaged above and below the thermocline from the summer survey,

232 averages throughout the water column were calculated from the winter data. Current velocities refer

233 to the resultant velocities calculated from the u and v component of the velocity vectors

234 (Supplementary Material 2 and 3) and were averaged over the time period of sampling. The current

235 data were provided by the *Bundesamt für Seeschifffahrt und Hydrographie* (BSH)

236 (www.bsh.de/de/Meeresdaten/Vorhersagen/Vorhersagemodelle/index.jsp), who model currents

237 using wind and air temperature forecasts.

238

239 If advective transport were to be uniform, then it would simply displace methane, but differences in

240 current velocity and direction with depth lead to turbulent mixing, i.e., eddy diffusion. The strength

241 of small-scale motions that act to smooth out concentration gradients can be parameterized by the

242 eddy diffusivity κ , such that mass transport is proportional to the mean concentration gradient

243 (Largier, 2003; Roberts and Webster, 2002):

244

245 $$Diff = \kappa \left(\frac{\partial C}{\partial x} \right) \tag{4}$$

246

247 where κ is the horizontal or vertical diffusion coefficient in $m^2\ s^{-1}$. $\delta C/\delta x$ is the spatial concentration

248 gradient in nM m^{-1}, estimated between the center and the outermost stations in the case of

249 horizontal diffusion calculation, and the concentration gradient between the lower and upper water

250 column in the case of vertical diffusion (Mau et al., 2012), calculated only for summer 2013.

251

252 κ_y, the horizontal diffusion coefficient, can range between 0.1 and 1000 $m^2\ s^{-1}$ (Largier, 2003;

253 Sundermeyer and Price, 1998) depending on the proximity to land. κ_y exponentially increases with

254 distance from the shore: κ_y is on the order of 1–10 $m^2\ s^{-1}$ if $y\sim0.1$ km, $\sim100\ m^2\ s^{-1}$ if $y\sim10$ km, and on

255 the order of 1000 $m^2\ s^{-1}$ or greater if $y\sim100–1000$ km. As the study area is located more than 230 km

256 from shore, we used a κ_y of 1000 $m^2\ s^{-1}$ for our calculations. The vertical turbulent diffusion

257 coefficient (κ_z) can vary between 10^{-3} and $10^{-6}\ m^2\ s^{-1}$ depending on the energy in the water column

258 (wind, tides, etc.) and stratification (Denman and Gargett, 1983; Wunsch and Ferrari, 2004). κ_z was

259 estimated according to the equation by Osborn (1980):

260

261 $$\kappa_z = \Gamma \frac{\epsilon}{N^2} \tag{5}$$

262

263 where Γ is the efficiency of mixing and assumed to be a constant of 0.2. We used published

264 dissipation rates of turbulent kinetic energy (ϵ) in stratified shallow shelf seas (Palmer et al., 2008;

265 Thorpe et al., 2008) and calculated the buoyancy frequency (N) from the available CTD-profiles. The

266 results indicate that κ_z is in the order of 10^{-4} to $10^{-6}\ m^2\ s^{-1}$ during stratification. This rough

267 approximation neglects hourly changes, which can vary by an order of magnitude. For example,

268 Palmer et al. (2008) observed and calculated κ_z to range between 10^{-4} and $10^{-5}\ m^2\ s^{-1}$ over a tidal

269 cycle. We used $10^{-4}\ m^2\ s^{-1}$, which is a common cited value across the thermocline, in order to not

270 underestimate the vertical eddy diffusion. This diffusion was estimated for all vertical profiles (all 10

271 CTD-stations).

272

273 The sea-air flux was calculated as:

274

275 $$SAF = k_W(C_W - C_A) \tag{6}$$

276

277 where k_W is the gas transfer velocity in cm h^{-1}, C_W is the measured concentration of methane and C_A

278 is the methane concentration in atmospheric equilibrium, both in nM. We calculated k_W, which

279 depends on wind speed and the temperature-dependent Schmidt number of the gas, using

280 parameterization developed by McGillis et al. (2001). Wind speed was recorded 22 m above sea level

281 onboard and corrected to the standard height of 10 m. C_A was derived using the mean atmospheric

282 methane concentration of Ocean Station M, Norway at 66°N and 2°E, in 2009 (1.874 ppm,

283 http://www.esrl.noaa.gov/gmd/dv/data/), the Bunsen solubilities given by Wiesenburg and Guinasso

284 (1979) and measured ocean temperature and salinities. The sea air flux was calculated for surface

285 water samples of all 10 stations sampled in summer 2013 and winter 2014.

286

287 The oxidative loss (OL) was calculated by depth integration of the MOx rates:

288

289 $$OL = \overline{x}_{MOx} z \qquad\qquad\qquad (7)$$

290

291 where $\overline{x}_{MOx}$ is the averaged MOx rate in nM day^{-1} over the depth interval z in m. The depth interval

292 is defined by the water stratification in the case of summer 2013 and covers the entire water depth

293 in the case of winter 2014. Integration was done for all vertical profiles.

294

295 3 Results

296 3.1 Seep locations

297 Echosounder data collected during the winter survey indicate bubble emission in the area of the

298 sampled transect (Fig. 2). The center station was located at a known gas bubble emission site or flare

299 cluster, where several bubble streams occur in close proximity to each other. We observed an

300 additional four flare clusters near the western sector of the transect, similar in seepage intensity as

301 those from the central seep denoted as cluster 1 (Fig. 2A and C). In contrast, no additional flares

302 were found in the area of the eastern sector. Although echosounder data point to bubbles rising to,

303 or close to, the sea surface, no bubbles were visually identified at the sea surface due to rough sea

304 state. Seepage intensity showed no obvious variation related to tidal cycles, i.e., pressure variations

305 due to high or low tides. The seeps were found to be active during all survey crossings. No

306 echosounder data were collected in summer 2013, nonetheless, surfacing gas bubbles were visually

307 documented when the sea was calm.

308

309 3.2 Oceanographic setting

310 In summer (July 2013) a seasonal thermocline separated surface (0-30 m) from bottom waters (30-42

311 m; Fig. 3). The surface water consisted of a 10 m thick mixed layer below which the temperature

312 decreased stepwise from 17.5 to 7°C in 30 m. Lower salinity was observed at 15 and 25 m depths,

313 which departed from the general value of 34.55. The stepwise decrease in temperature and the

314 salinity variations indicate the successive development of several pycnoclines driven by increasing

315 sea surface temperatures and ~~less~~ wind activity in spring and summer. The oxygen concentrations

316 increased from 220 µM at the surface to 240 µM at 30 m. In contrast to the surface water, the

317 bottom water had a homogeneous temperature of 7°C, a salinity of 34.63 and contained less oxygen

318 (190 µM).

319

320 In winter (January 2014) the entire water column was mixed (Fig. 3). The water had a temperature of

321 7°C, a salinity of 34.85, a density of 27.3 kg m^{-3}, and oxygen concentrations of 280 µM.

322

323 Modeled regional current data provided by the BSH indicate a dominant north-west transport

324 throughout the water column with surface velocities ranging between 0.0? and 0.27 m s^{-1} (resultant

325 velocity). In summer, the eastern part of the transect was sampled when currents were directed to

326 the north-west with an average velocity of 0.24 m s^{-1} and the western part was sampled when

327 currents turned from north-west to south-west with an average velocity of 0.19 m s^{-1}. In winter, the

328 eastern part of the transect was sampled when water moved north-east turning north-west with an

329 average velocity of 0.22 m s^{-1} and the western part was sampled when water also turned from north-

330 east to north-west, but with an average velocity of 0.1 m s^{-1}. Water velocity and direction plots are

331 given in Supplementary Material 2 and 3.

332

333 3.3 Methane concentrations

334 Consistent with the two layer structure observed on the hydrographic data, the methane

335 concentration in summer 2013 also show a two layer distribution, with higher values in the bottom

336 water (Fig. 4A, Supplementary Material 4). Methane concentrations in the surface water range from

337 3.9-517.8 nM with a median of 32.5 nM. Methane concentrations in the bottom water range

338 between 39.7 and 1627.7 nM with a median of 390.6 nM. Highest concentrations in the surface

339 water were found near cluster 1 (170 nM) and generally decreased towards the outermost stations

340 (to the west to 96 nM and to the east to 13 nM). Similarly, in the bottom water the highest methane

341 concentrations were found at cluster 1 (600-700 nM), and concentrations decreased unevenly

342 towards the outmost stations (200-300 nM). In both layers the methane concentrations exceed the

343 background concentration of ~20 nM as measured at a reference station located 32 km to the south-

344 east of cluster 1 (Supplementary Material 5), and those reported by Grundwald et al. (2??). Even

345 this regional background value is supersaturated with respect to the atmospheric equilibrium

346 concentration of 2.3-2.9 nM (at the relevant T/S conditions, Wiesenburg and Guinasso, 1979).

347

348   Much lower methane concentrations were found in winter 2014 (Fig. 4B, Supplementary Material 4).

349   Highest values were observed only at one station near cluster 1 with concentrations reaching 656.6

350   nM. Such elevated values decreased rapidly horizontally (within 1 km) and were not encountered

351   during repeated hydrocasts at the same location. The median of all methane concentration

352   measurements along the transect was 22.4 nM, which is only slightly above the regional background

353   concentration. In general, methane concentrations indicate a patchy distribution as expected in an

354   active seep area.

355

356   3.4 UWMS methane concentrations

357   The UWMS was deployed in the vicinity of flare cluster 1 in summer 2013 covering an area of 125 m

358   by 150 m during instrument tow (Fig. 2C). Therefore, the hydrocast data (described in section 3.3)

359   cover a much larger spatial scale sampled during the UWMS-tows. When the UWMS was towed close

360   to bubble streams, it recorded methane concentrations ranging over three orders of magnitude,

361   from <16 nM (the detection limit, which is recorded as 0) to 2127 nM in surface waters (transects in

362   10 m, 25 m, 28 m), but values > 500 nM were only recorded during a period of ~11 min of the ~30

363   min tow at 25 m and ~4 min of the ~60 min tow at 28 m (Fig. 5). During bottom transects (30 m and

364   42 m) methane concentration are generally higher, ranging from 259 to 2213 nM. The median values

365   of the records from the 10 m, 25 m, and 28 m water depth tows were <16 nM, 133 nM, and 158 nM,

366   respectively, while the median in 30 m and 40 m depth were 508 and 679 nM.

367

368   The UWMS tows were conducted during ebbing tides, when water levels fell from 0.18 to -0.27 m,

369   whereas hydrocast samples were collected during rising tides, when sea level height increased from -

370   0.21 to 0.06 m and from 0.04 to 0.16 m (Supplementary Material 6). The general pattern of lower

371   concentrations in the surface and higher ones in the bottom water was apparent in all stations, even

372   though methane data were obtained using different techniques and samples were collected during

373   different tidal phases.

374

375   3.5 Methane oxidation

376   Similar to the distribution of methane and co-located oceanographic data, the MOx rates calculated

377   using equation (1) show a two layer pattern in summer 2013, but are uniform throughout the water

378   column during the winter 2014 survey (Fig. 6A). In summer, MOx-rates in surface waters ranged

379   between 0.04 and 9.17 nM day^{-1} with a median of 0.10 nM day^{-1} and in the bottom water between

380   1.60 and 840.93 nM day^{-1} with a median of 3.99 nM day^{-1}. The total range of both layers (0.04-

381   840.93 nM day^{-1}) exceeds the range of MOx-rates observed during the winter survey (0.09-8.72 nM

382   day^{-1}). The median of all MOx-rates measured in January 2014 was 0.24 nM day^{-1}.

383

384 3.6 Microbial communities

385 Molecular samples taken in summer 2013 show also a difference between surface and deep waters,

386 whereas winter 2014 samples indicate a homogeneous distribution of microorganisms (Fig. 7, Tab.

387 1). In summer 2013, different DGGE banding patterns reveal changes in microbial communities with

388 depth. The surface water samples showed two strong bands (Fig. 7, bands 6, 7) that could be

389 affiliated to the *Rhodobacteraceae* and two bands that could be assigned to the *Cyanobacteria /*

390 *Synechococcus* clade (8, 9). The middle and bottom water samples were characterized by a strong

391 chloroplast band (2), but also showed bands affiliated to the *Rhodobacteraceae* (5, 6). In the bottom

392 water samples of the central station, we found an additional band, assigned to *Pseudoalteromonas*

393 (10). The gel pattern of the winter samples showed no significant bands. The sequences of the faint

394 bands excised were of low quality. Only two of the bands could be assigned to the *Rhodospirillaceae*

395 (12, 13).

396

397 Neither the summer nor the winter bacterial communities exhibited known methanotrophic

398 bacteria, even though the samples originate from an actively gas venting area. The absence of

399 methanotrophic bacteria was further supported by the negative results of the *pmoA*-PCRs that

400 targets a methanotroph molecular marker gene.

401

402 4 Discussion

403 The echosounder and visual observations at the central North Sea sites document gas emissions that

404 in some cases reach the sea surface. This fraction of methane that is transported directly to the

405 atmosphere by ~~bursting~~ bubbles might be ~~crucial,~~ as was shown for example at the shallow seep field

406 Coal Oil Point in California (<70 m) where about half of the methane is directly emitted to the

407 atmosphere via ~~bursting~~ bubbles and the other half is injected in the water (Clark et al., 2000).

408 ~~However,~~ we focus on the dissolved methane fraction that remains in the in the ocean and ~~can be~~

409 microbially ~~oxidized.~~

410

411 4.1 Distribution of methane in summer and winter

412 Our highest dissolved methane concentrations, measured in the bottom water during the summer

413 survey, reach magnitudes similar to those observed at other shallow seep sites (Tab. 2). Our highest

414 value of 1627.7 nM is comparable to measurements near the Coal Oil Point seep field (up to 1900

415 nM, Mau et al., 2012), and it is higher than methane concentrations reported for seep locations in

416 the Tommeliten, North Sea (268 nM, Schneider von Deimling et al., 2011), and offshore Svalbard,

417 west of Prins Karls Forland (524 nM, Gentz et al., 2013).

418

419   Even though gas bubbling was observed at the sea surface during the summer survey, the dissolved

420   methane appears trapped beneath the seasonal thermocline (Fig. 4A). This observation is similar to

421   those at the Tommeliten site, where the dissolved methane plume was sequestered beneath the

422   seasonal thermocline (Schneider von Deimling et al., 2011) although gas flares were imaged to rise

423   within 10 m of the sea surface. Elevated methane concentrations at other vent sites have also been

424   reported beneath a thermocline or halocline that hamper further ascent of dissolved methane to the

425   mixed layer. The dissolved methane plume originating from the 245 m deep seeps offshore Prins

426   Karls Forland was confined to water depths beneath a local halocline (Gentz et al., 2013). In the Baltic

427   Sea, summer stratification also leads to accumulation of methane below the thermocline (Gülzow et

428   al., 2013). At all these sites, an enhanced release of methane to the atmosphere is thought to occur

429   upon erosion of stratification. In contrast, the dissolved methane plume originating from seeps

430   situated between 5 and 70 m at the Coal Oil Point is dispersed within the mixed layer above the

431   thermocline (Mau et al., 2012), and as such it is not controlled by seasonal stratification patterns.

432

433   Trapping and accumulation of dissolved methane beneath a thermocline is also well documented in

434   lakes and freshwater reservoirs, where thermal stratification separates methane-poor, surface water

435   from the methane-rich, but anoxic, bottom water in e.g. a shallow floodplain lake in south-eastern

436   Australia (Ford et al., 2002), in a polyhumic lake in southern Finland (Kankaala et al., 2007), in the

437   subtropical Lake Kinneret in Israel (Eckert and Conrad, 2007), and in 8 freshwater reservoirs in India

438   (Narvenkar et al., 2013). The accumulated methane is released to the atmosphere at the onset of

439   water column mixing in response to enhanced wind forcing and lower temperatures.

440

441   Our results show that in a seasonal stratified system, no methane accumulation occurs in winter,

442   when the water column is well mixed (Fig. 4B). Methane concentrations were found to deviate only

443   due to bubble ascent and were otherwise low and constant throughout the water. The median

444   winter concentration of 22 nM is similar to the background values of 20 nM reported by Grunwald et

445   al. (2009) for the German Bight, but is elevated relative to water originating from the Atlantic Ocean,

446   which carries 2.5-3.5 nM of methane (Rehder et al., 1998) and to the methane background

447   concentrations of <5 nM at Tommeliten (Niemann et al., 2005; Schneider von Deimling et al., 2011).

448

449   The observed difference between summer and winter dissolved methane concentrations may also be

450   due to changes in seepage rate. The visual observation of gas bubbles during the summer, Schroot et

451   al.'s (2005) sub-bottom profiler recording of gas plumes in the water column in August 2002, and our

452   acoustic records of gas flares in the winter (Fig. 2B) indicate that seepage occurred during both

453 seasons. Notwithstanding these observations, we recognize that we ~~do not~~ have ~~enough~~ temporal

454 data coverage and that bubble release frequency, bubble size and initial methane content could ~~still~~

455 have been different between our surveys causing the difference in overall methane concentrations

456 (Greinert and McGinnis, 2009; Leifer and Clark, 2001; McGinnis et al., 2006). However, even when a

457 change in seepage regimes could affect the overall methane concentration, it would not explain the

458 difference in the methane profiles observed between summer and winter surveys.

459

460 Discrete sampling bias and current~~s~~ variability ~~may~~ also explain the difference observed between

461 summer and winter dissolved methane concentrations. The currents had a strong westward

462 component during summer sampling with small north/south deviation throughout the water column

463 (Supplementary Material 2), and thus the easternmost profiles are likely to be less influenced from

464 direct bubble seepage (Fig. 4A). However, the profiles still show elevated methane concentration in

465 the bottom water and lower concentrations in the shallow samples, consistent with methane

466 trapping below the seasonal thermocline. We considered whether the low observed concentrations

467 during winter may be due to the fact that during this survey we only partially sampled isolated

468 plumes. Although the east-west-transect directly crust the cluster 1 flares (Fig. 2) and was oriented in

469 direction of the tidal movement in that area, the stronger northward component of the current in

470 winter (Supplementary Material 2 and 3) displaced methane plumes more rapidly than in summer.

471 The elevated methane concentrations at the central seep site and along the western transect

472 (although with much lower methane concentrations) suggest that we indeed sampled methane

473 plumes (Fig. 4B). We note that the horizontal concentration gradient in surface water were 0.01 to

474 0.02 nM m^{-1} during summer and winter, respectively. As a first order approximation we take the

475 highest concentration measured (39 in summer and 73 nM in winter) and a general current speed of

476 0.2 m s^{-1} to estimate a plume size of ~4 km in diameter that would take ~5 h to cross our sampling

477 transect. Since we always sampled 5 stations in ~3 h for the eastern or western segments of the

478 transect, it seems rather unlikely that we completely missed a methane plumes.

479

480 To summarize, even when methane concentrations may appear biased by discrete sampling, current

481 differences, and seepage rate, our data analyses suggest that the seasonal differences are real. Even

482 if the total magnitudes may be questioned, we are confident that the methane distribution pattern is

483 the result of seasonal stratification.

484

485 4.2 Interpreting methane oxidation rate data

486 Measured MOx-rates at our study site (Fig. 6A) lie at the upper end of MOx-rates previously reported

487 at sites elsewhere, which span over six orders of magnitude from 0.001-1000 nM day^{-1} (Tab. 2 and

488   summarized in Fig. 1 in Mau et al., 2013). The rates measured in deep water samples during summer

489   (median 3.9 nM day^{-1}, up to 840 nM day^{-1}) equal those observed in the Gulf of Mexico after the

490   Deepwater Horizon event (median 10 nM d^{-1}, up to 820 nM day^{-1}) (Valentine et al., 2010). Even in

491   winter time, the estimated rates are high in comparison to those measured in the Eel River Basin, an

492   area of documented gas hydrate dissociation (Valentine et al., 2001) and match rates of the Coal Oil

493   Point seep field in the Santa Barbara Basin (Mau et al., 2012; Pack et al., 2011).

494

495   In spite of the reported high MOx values, our data reveal an overall low activity of methane oxidizing

496   microorganisms based on the values obtained for the rate constant *k'*, which provides an indication

497   of the relative activity in a water sample (Koschel, 1980). This is a first-order constant if the reaction

498   is solely dependent on the methane concentration and biomass does not increase during incubation.

499   Our experiments yielded similar *k'* values over a wide range of methane concentrations spanning

500   from 4 to 728 nM (Fig. 6C). Furthermore, the good correlation between methane oxidation rates and

501   methane concentration (Fig. 6D) indicate that the biomass did not increase during incubation, thus

502   validating our inferences on microbial activity based on *k'* values. Based on 116 (out of 123)

503   measurements we calculate an average value for *k'* of 0.01 day^{-1}, i.e., a turnover time of 100 days

504   (Fig. 6B). This value matches the value *k'* derived from our time series incubation results (0.01 day^{-1},

505   n=4), which show that only 5-6% of the added ^{3}H-methane tracer was consumed by microbial activity

506   after 4 incubation days (Supplementary Material 7). The time series show a linear increase of tracer

507   oxidation and the function derived from Fig. 6D that yield a first-order relationship between methane

508   oxidation rates and methane concentration with *k'*=0.01. If we use the average *k'* and methane

509   concentrations that span 4-728 nM, the resulting oxidation rates (Eq. 1) range between 0.04-7.28 nM

510   day^{-1}. Thus relatively high MOx-rates here reflect primarily high methane concentrations, and must

511   not be taken as indication of a high microbial turnover.

512

513   We note that 7 data points collected in summer near flare cluster 1 (stations 12 and 13) had *k'* values

514   ranging from 0.08 to 0.64 day^{-1}, significantly higher than the rest of the measurements. These high

515   values multiplied with high corresponding methane concentrations gave the highest MOx-values

516   measured during this study. These elevated *k'* values may indicate an increase in biomass and/or an

517   increase in activity of the methane oxidizing community in the water sample during incubation.

518

519   The general low activity of methane oxidizing microorganisms is further supported by molecular

520   analysis of filtered matter from seawater. Consistently, DGGE and *pmoA* analysis did not reveal the

521   presence of any known methanotrophic bacteria or *pmoA*-genes. Either methanotrophs were only

522   present in low numbers and/or poorly matched to the used PCR primers and, thus, were not

523 detected (Hansman, 2008). We also note that although no canonical methanotrophs were detectable

524 in shallow marine waters (< 200 m) in the Pacific, Atlantic, and the Gulf of Mexico, further analyses of

525 these samples revealed sequences closely related to those coding for methane monooxygenase

526 (Elsaied et al., 2004; Tavormina et al., 2008; Tavormina et al., 2013; Valentine, 2011; Wasmund et al.,

527 2009), an enzymatic hallmark of aerobic methanotrophs. We recognize that not having detected

528 methanotrophs in our samples does not preclude their presence in the water column.

529

530 Even though during summer stratification methane is trapped beneath the seasonal thermocline, the

531 resulting higher methane concentrations do not appear to enhance the activity of methane oxidation

532 microbes. The residence time of central North Sea water is about 1.5-2 years (Prandle, 1984; Ursin

533 and Andersen, 1978) and thermal stratification prevails for 4 months, which may provide sufficient

534 time to establish a methanotrophic community. However, microbial turnover times in bottom water

535 samples are consistently low and we were not able to identify methanotrophic organisms in the

536 water column. Doubling times of planktonic marine methanotrophs are not known to the authors,

537 but if we assume a doubling time of ~10 h as known from cultured methanotrophs (Baani and

538 Liesack, 2008; Khadem et al., 2010) or a doubling time of 3.5 days estimated after the Deep Water

539 Horizon incident in the Gulf of Mexico (Kessler et al. (2011), a methanotrophic community could

540 potentially develop in the central North Sea during the 4 months where stratification leads to

541 enhanced methane content in the bottom water. Even if the doubling time of methanotrophs in the

542 field was longer than in culture as nutrients and substrates can be limiting, the residence time of the

543 water would permit growth. Possible limitations may be a lack of essential trace elements or that the

544 methane oxidizing microorganisms are facultative methanotrophs (Tavormina et al., 2013), i.e., not

545 necessarily depending on methane.

546

547 In summary, even though total MOx rates are necessary to constrain overall methane budgets and

548 carbon cycles, to better characterize microbial activity among different ecosystems it is necessary to

549 also report data on the microbial turnover rates at each site. The low turnover rates measured here

550 are consistent with molecular analyses that failed to identify methanotrophic bacteria or *pmoA*-

551 genes. Enhanced methane concentrations do not appear to foster higher turnover rates.

552

553 4.3 Methane transport in the North Sea is faster than oxidation

554 When methane enters the water column, either directly from the seep or by dissolution/gas

555 exchange from ascending bubbles, it is transported by ocean currents and spreads by horizontal and

556 vertical eddy diffusion. Methane oxidizing microorganisms can consume dissolved methane in the

557 water column, and methane will be transferred into the atmosphere if its concentration in the mixed

558 layer is higher than saturation.

559

560 As a first order evaluation of the relative importance of these transport and loss processes, we

561 estimated the advective transport, the horizontal and vertical eddy diffusion, sea-air flux, and

562 integrated the MOx-rates (see methods and Mau et al., 2012). Summer fluxes for the bottom (30-

563 43m) and surface waters (0-30 m), were estimated using data collected in July 2013, and winter

564 fluxes were derived for the entire unstratified water column (0-42m) using data from January 2014.

565 All fluxes were estimated in units of nmol $m^{-2} s^{-1}$. These flux estimates may vary by up to one order of

566 magnitude due to measurement errors, assumed diffusion coefficients and parameterization of the

567 gas transfer velocity. A detailed discussion of the uncertainties associated with the calculations is

568 given by Mau et al. (2012).

569

570 The results shown in Fig. 8 revealed that in both summer and winter seasons, horizontal advection

571 and eddy diffusion are the dominant processes transporting and diluting the emitted methane. The

572 loss processes, i.e., sea air flux and microbial oxidation, are more than 4-orders of magnitude lower

573 than physical horizontal transport processes.

574

575 Vertical mixing due to internal waves resulting from proximity to the elevation of the Dogger Bank

576 cannot be ruled out. Estimates of κ_z for the shelf break range in the order of $0.5-0.7\cdot10^{-4} m^2 s^{-1}$

577 (Palmer et al., 2008). Our vertical fluxes based on $\kappa_z =10^{-4} m^2 s^{-1}$, thus include the enhanced mixing by

578 internal waves that support increased transport across the seasonal thermocline.

579

580 Sea-air flux estimates depend on variations in the atmospheric methane concentration. We don't

581 have data on atmospheric methane variations directly over our study site; however, if we consider

582 published variations at other seep sites (e.g. 1.71-3.83 ppm above seeps in the northern Gulf of

583 Mexico, Hu et al., 2012), our estimates are correct within the order of magnitude range stated as our

584 uncertainty. Not surprisingly, the sea-air flux removes more methane from the water column during

585 winter due to increased wind speed. More unexpectedly, our flux estimates revealed that in summer

586 the amount of methane that is transported via vertical diffusion into the surface water is of similar

587 magnitude than the loss by oxidation in the bottom water, even water stratification leads to

588 enhanced methane concentrations at depth. In summer, when lower wind speeds prevail, methane

589 oxidation was estimated to be of similar magnitude as the gas transfer to the atmosphere.

590

591 Our findings are similar to those reported by Scranton and McShane (1991) for the Southern Bight of

592 the North Sea. They conclude that methane oxidation constitutes a relatively small sink for methane

593 (0.00023-0.3 nM day^{-1}), relative to methane losses to the atmosphere (0.00026-7.5 nM day^{-1}), which

594 are highest during periods of high wind speed. Similarly, estimates for the shallow Coal Oil Point

595 methane plume in the Santa Barbara Basin (Mau et al., 2012) show that at this location 0.05 mol day^{-}

596 ^{1} are oxidized in the surface water and 0.03 mol day^{-1} are transferred to the atmosphere.

597

598 5 Conclusions

599   1.   Observations at a shallow gas seep site in the central North Sea document methane

600   accumulation below the thermocline during summer stratification, but no methane

601   accumulation in the winter when water column is well mixed.

602   2.   At our study site, physical transport processes always outcompete microbial methane

603   oxidation. Horizontal advection and diffusion of methane are consistently higher than

604   vertical transport, even within order of magnitude uncertainties. During periods of high wind

605   speed (fall and winter), more methane reaches the atmosphere than is oxidized in the water;

606   in summer the loss to the atmosphere and the oxidation terms are of similar magnitude.

607   3.   We show that MOx rates alone cannot be used to characterize the ecosystem microbial

608   activity, as these values are scaled to the methane concentration. We instead propose to

609   include interpretation of k' values as an indicator of microbial activity. Averaged k' values

610   generate a more realistic parameter than values based solely on replicate samples as further

611   documented by our work-intensive time series incubations.

612   4.   Our results demonstrate that trapping of methane below a seasonal thermocline does not

613   necessarily lead to enhance microbial oxidation. Further research is needed to elucidate why

614   stratification over a summer season of 4 months does not enhance methanotrophy enough

615   to significantly hamper methane release to the atmosphere upon water column mixing.

616

617

618

619

620

621

622

623

624

625

626 Author contribution

627 S. M. designed study, measured methane concentrations and methane oxidation rates, calculated

628 the fluxes, wrote the manuscript

629 T.G., R. M., and M.S. deployed the UWMS and post-processed the data

630 J.-H. K., M. R., H. S., and P. W. collected and post-processed hydroacoustic data

631 M. T. interpreted methane oxidation rate data, edited manuscript

632 E. H. implemented and interpreted molecular analyses

633

634

635

636

637

638

639

640

641

642

643

644

645

646

647

648

649

650

651

652

653

654

655

656

657

658

659

660

671

672

673

674

675

676

677

678

679

680

681

682

683

684

685

686

687

688

689

690

691

692

693

694

695

696   References

697   Baani, M. and Liesack, W.: Two isozymes of particulate methane monooxygenase with different

698   methane oxidation kinetics are found in Methylocystis sp. strain SC2, PNAS, 105, 10203-10208, 2008.

699   Bange, H. W.: Nitrous oxide and methane in European coastal waters, Estuar. Coast. Shelf S., 70, 361-

700   374, 2006.

701   Bange, H. W., Bartell, U. H., Rapsomanikis, S., and Andreae, M. O.: Methane in the Baltic and North

702   Seas and a reassessment of the marine emissions of methane, Global Biogeochem. Cy., 8, 465-480,

703   1994.

704   Bell, R. J., Short, R. T., Van Amerom, F. H. W., and Byrne, R. H.: Calibration of an in situ membrane

705   inlet mass spectrometer for measurements of dissolved gases and volatile organics in seawater,

706   Environ. Sci. Technol., 41, 2007.

707   Berner, R. A.: Biogeochemical cycles of carbon and sulfur and their effect on atmospheric oxygen

708   over Phanerozoic time, Palaeogeogr. Palaeocl., 73, 97-122, 1989.

709   Boetius, A., Ravenschlag, K., Schubert, C. J., Rickert, D., Widdel, F., Gieskes, A., Amann, R., Jørgensen,

710   B. B., Witte, U., and Pfannkuche, O.: A marine microbial consortium apparently mediating anaerobic

711   oxidation of methane, Nature, 407, 623-626, 2000.

712   Cicerone, R. J. and Oremland, R. S.: Biochemical aspects of atmospheric methane, Global

713   Biogeochem. Cy., 2, 299-327, 1988.

714   Denman, K. L. and Gargett, A. E.: Time and space scales of vertical mixing and advection of

715   phytoplankton in the upper ocean, Limnol. Oceanogr., 28, 801-815, 1983.

716   Eckert, W. and Conrad, R.: Sulfide and methane evolution in the hypolimnion of a subtropical lake: a

717   three-year study, Biogeochemistry, 82, 67-76, 2007.

718   Elsaied, H. E., Hayashi, T., and Naganuma, T.: Molecular analysis of deep-sea hydrothermal vent

719   aerobic methanotrophs by targeting genes of 16S rRNA and particulatemethane monooxygenase,

720   Mar. Biotechnol., 6, 503–509, 2004.

721   Etiope, G., Lassey, K. R., Klusman, R. W., and Boschi, E.: Reappraisal of the fossil methane budget and

722   related emission from geologic sources, Geophys. Res. Lett., 35, L09307, 2008.

723   Ford, P. W., Boon, P. I., and Lee, K.: Methane and oxygen dynamics in a shallow floodplain lake: the

724   significance of period stratification, Hydrobiologia, 485, 97-110, 2002.

725   Gentz, T., Damm, E., Schneider von Deimling, J., Mau, S., McGinnis, D. F., and Schlüter, M.: A water

726   column study of methane around gas flares located at the West Spitsbergen continental margin,

727   Cont. Shelf Res., doi: 10.1016/j.csr.2013.07.013, 2013. 2013.

728   Gentz, T. and Schlüter, M.: Underwater cryotrap-membrane inlet system (CT-MIS) for improved in

729   situ analysis of gases, Limnol. Oceanogr.: Methods, 10, 317-328, 2012.

730 Gerdes, B., Brinkmeyer, R., Dieckmann, G., and Helmke, E.: Influence of crude oil on changes of

731 bacterial communities in Arctic sea-ice, FEMS Microbiol. Ecol., 53, 129-139, 2005.

732 Greinert, J. and McGinnis, D. F.: Single bubble dissolution model - The graphical user interface SiBu-

733 GUI, Environ. Model. Softw., 24, 1012-1013, 2009.

734 Grunwald, M., Dellwig, O., Beck, M., Dippner, J. W., Freund, J. A., Kohlmeier, C., Schnetger, B., and

735 Brumsack, H.-J.: Methane in the southern North Sea: Sources, spatial distribution and budgets,

736 Estuar. Coast. Shelf S., 81, 445-456, 2009.

737 Gülzow, W., Rehder, G., Schneider v. Deimling, J., Seifert, T., and Tóth, Z.: One year of continuous

738 measurements constraining methane emissions from the Baltic Sea to the atmosphere using a ship of

739 opportunity, Biogeosciences, 10, 81-99, 2013.

740 Holt, J. and Umlauf, L.: Modelling the tidal mixing fronts and seasonal stratification of the Northwest

741 European Continental shelf, Cont. Shelf Res., 28, 887-903, 2008.

742 Howarth, M. J.: North Sea Circulation. In: Encyclopedia of Ocean Sciences, Steele, J. H. (Ed.),

743 Academic Press, Oxford, 2001.

744 Hu, L., Yvon-Lewis, S. A., Kessler, J. D., and MacDonald, I. R.: Methane fluxes to the atmosphere from

745 deepwater hydrocarbon seeps in the northern Gulf of Mexico, J. Geophys. Res., 117, 2012.

746 IPCC: Climate Change 2013 – The Physical Science Basis – Contribution of Working Group I to the

747 Fifth Assessment Report of the Intergovernmental Panel on Climate Change, Cambridge University

748 Press, Cambridge, 2013.

749 Jørgensen, B. B. and Kasten, S.: Sulfur Cycling and Methane Oxidation. In: Marine Geochemistry,

750 Schulz, H. D. and Zabel, M. (Eds.), Springer, Berlin Heidelberg 2006.

751 Kankaala, P., Taipale, S., Nykänen, H., and Jones, R. I.: Oxidation, efflux, and isotopic fractionation of

752 methane during autumnal turnover in a polyhumic, boreal lake, J. Geophys. Res., 112, G02003, 2007.

753 Kessler, J. D., Valentine, D. L., Redmond, M. C., Du, M., Chan, E. C., Mendes, S. D., Quiroz, E. W.,

754 Villanueva, C. J., Shusta, S. S., Werra, L. M., Yvon-Lewis, S. A., and Weber, T. C.: A persistent oxygen

755 anomaly reveals the fate of spilled methane in the deep Gulf of Mexico, Science, 331, 312-315, 2011.

756 Khadem, A. F., Pol, A., Jetten, M. S. M., and Op den Camp, H. J. M.: Nitrogen fixation by the

757 verrucomicrobial methanotroph '*Methylacidiphilum fumariolicum*' SolV, Microbiology, 156, 1052-

758 1059, 2010.

759 Killops, S. D. and Killops, V. J.: An Introduction to Organic Geochemistry, Longman, Essex, United

760 Kingdom, 1993.

761 King, G. M.: Ecological aspects of methane oxidation, a key determinant of global methane dynamics,

762 Adv. Microb. Ecol., 12, 432-468, 1992.

763 Koschel, R.: Untersuchungen zur Phosphataffinitat des Planktons in der euphotischen Zone von Seen,

764 Limnologica, 12, 141-145, 1980.

765 Kröncke, I. and Knust, R.: The Dogger Bank: a special ecological region in the central North Sea,

766 Helgoländer Meeresunters., 49, 335-353, 1995.

767 Largier, J. L.: Considerations in estimating larval dispersal distances from oceanographic data, Ecol.

768 Appl., 13, 71-89, 2003.

769 Leifer, I. and Clark, J.: Modeling trace gases in hydrocarbon seep bubbles. Application to marine

770 hydrocarbon seeps in the Santa Barbara Channel, Russ. Geol. Geophys., 43, 613-621, 2001.

771 Magen, C., Lapham, L. L., Pohlman, J. W., Marshall, K., Bosman, S., Casso, M., and Chanton, J. P.: A

772 simple headspace equilibration method for measuring dissolved methane, Limnol. Oceanogr. Meth.,

773 12, 637–650, 2014.

774 Mau, S., Blees, J., Helmke, E., Niemann, H., and Damm, E.: Vertical distribution of methane oxidation

775 and methanotrophic response to elevated methane concentrations in stratified waters of the Arctic

776 fjord Storfjorden (Svalbard, Norway), Biogeosciences, 10, 6267–6278, 2013.

777 Mau, S., Heintz, M. B., and Valentine, D. L.: Quantification of CH_4 loss and transport in dissolved

778 plumes of the Santa Barbara Channel, California, Cont. Shelf Res., 32, 110-120, 2012.

779 McDonald, I. R., Bodrossy, L., Chen, Y., and Murrell, J. C.: Molecular ecology techniques for the study

780 of aerobic methanotrophs, Appl. Environ. Microb., 74, 1305-1315, 2008.

781 McDonald, I. R. and Murrell, J. C.: The particulate methane monooxygenase gene pmoA and its use as

782 a functional gene probe for methanotrophs, FEMS Microbiol. Lett., 156, 205-210, 1997.

783 McGillis, W., R., Edson, J., B., Ware, J., D., Dacey, J., W. H., Hare, J., E., Fairall, C., W., and Wanninkhof,

784 R.: Carbon dioxide flux techniques performed during GasEx-98, Mar. Chem., 75, 267-280, 2001.

785 McGinnis, D. F., Greinert, J., Artemov, Y., Beaubien, S. E., and Wuest, A.: Fate of rising methane

786 bubbles in stratified waters: How much methane reaches the atmosphere?, J. Geophys. Res., 111, 15,

787 2006.

788 Muyzer, G., de Waal, E., and Uitterlinden, A.: Profiling of complex microbial populations by

789 denaturing gradient gel electrophoresis analysis of polymerase chain reaction-amplified genes coding

790 for 16S rRNA, Appl. Environ. Microbiol., 59, 695-700, 1993.

791 Narvenkar, G., Naqvi, S. W. A., Kurian, S., Shenoy, D. M., Pratihary, A. K., Naik, H., Patil, S., Sarkar, A.,

792 and Gauns, M.: Dissolved methane in Indian freshwater reservoirs, Environ. Monit. Assess., 185,

793 6989–6999, 2013.

794 Niemann, H., Elvert, M., Hovland, M., Orcutt, B., Judd, A. G., Suck, I., Gutt, J., Joye, S., Damm, E.,

795 Finster, K., and Boetius, A.: Methane emission and consumption at a North Sea gas seep (Tommeliten

796 area), Biogeosciences 2, 335-351, 2005.

797 Niewöhner, C., Hensen, C., Kasten, S., Zabel, M., and Schulz, H. D.: Deep sulfate reduction completely

798 mediated by anaerobic methane oxidation in sediments of the upwelling area off Namibia, Geochim.

799 Cosmochim. Ac., 62, 455-464, 1998.

800   Osborn, T. R.: Estimates of the local rate of diffusion from dissipation measurements, J. Phys.

801   Oceanogr., 10, 83-89, 1980.

802   Otto, L., Zimmermann, J. T. F., Furnes, G. K., Mork, M., Saetre, R., and Becker, G.: Review of the

803   physical oceanography of the North Sea, Neth. J. Sea Res., 26, 161-238, 1990.

804   Pack, M. A., Heintz, M. B., Reeburgh, W. S., Trumbore, S. E., Valentine, D. L., Xu, X., and Druffel, E. R.

805   M.: A method for measuring methane oxidation rates using low-levels of ^{14}C-labeled methane and

806   accelerator mass spectrometry, Limnol. Oceanogr.: Methods, 9, 245-260, 2011.

807   Palmer, M. R., Rippeth, T. P., and Simpson, J. H.: An investigation of internal mixing in a seasonally

808   stratified shelf sea, J. Geophys. Res., 113, 2008.

809   Pingree, R. D. and Griffiths, D. K.: Tidal Fronts on the Shelf Seas Around the British Isles, J. Geophys.

810   Res., 83, 4615-4622, 1978.

811   Prandle, D.: A modelling study of the mixing of ^{137}Cs in the seas of the European continental shelf,

812   Philos. T. Roy. Soc. A 310, 407-436, 1984.

813   Pruesse, E., Peplies, J., and Glöckner, F. O.: SINA: accurate high-throughput multiple sequence

814   alignment of ribosomal RNA genes, Bioinformatics, 28, 1823-1829, 2012.

815   Reeburgh, W. S., Ward, B. B., Whalen, S. C., Sandbeck, K. A., Kilpatrick, K. A., and Kerkhof, L. J.: Black

816   Sea methane geochemistry, Deep-Sea Res., 38, S1189-S1210, 1991.

817   Rehder, G., Keir, R. S., Suess, E., and Pohlmann, T.: The multiple sources and patterns of methane in

818   North Sea waters, Aquat. Geochem., 4, 403-427, 1998.

819   Roberts, P. J. W. and Webster, D. R.: Turbulent Diffusion. In: Environmental Fluid Mechanics-Theories

820   and Application, Shen, H., Cheng, A., Wang, K.-H., Teng, M. H., and Liu, C. (Eds.), Amer. Soc. Civil Eng.

821   Press, Reston, Virginia, 2002.

822   Schlüter, M. and Gentz, T.: Application of membrane inlet mas spectrometry for online and in situ

823   analysis of methane in aquatic environments, J. Am. Soc. Mass Spectrom., 19, 1395-1402, 2008.

824   Schneider von Deimling, J., Rehder, G., Greinert, J., McGinnis, D. F., Boetius, A., and Linke, P.:

825   Quantification of seep-related methane gas emissions at Tommeliten, North Sea, Cont. Shelf Res., 31,

826   876-878, 2011.

827   Schroot, B. M., Klaver, G. T., and Schuettenhelm, T. E.: Surface and subsurface expressions of gas

828   seepage to the seabed - examples from the southern North Sea, Mar. Petrol. Geol., 22, 499-515,

829   2005.

830   Scranton, M. I. and McShane, K.: Methane fluxes in the southern North Sea: The role of European

831   rivers, Cont. Shelf Res., 11, 37-52, 1991.

832   Short, R. T., Fries, D. P., Kerr , M. L., Lembke, C. E., Toler, S. K., Wenner, P. G., and Byrne, R. H.:

833   Underwater mass spectrometers for in situ chemical analysis of the hydrosphere, J. Am. Soc. Mass

834   Spectrom., 12, 676-682, 2001.

835 Sundermeyer, M. A. and Price, J. F.: Lateral mixing and the North Atlantic tracer release experiment:

836 observations and numerical simulations of Lagrangian particles and a passive tracer, J. Geophys. Res.,

837 103, 21481-21497, 1998.

838 Sündermann, J. and Pohlmann, T.: A brief analysis of North Sea physics, Oceanologia, 53, 663-689,

839 2011.

840 Tavormina, P. L., Ussler III, W., and Orphan, V. J.: Planktonic and sediment-associated aerobic

841 methanotrophs in two seep systems along the North American Margin, Appl. Environ. Microbiol., 74,

842 3985-3995, 2008.

843 Tavormina, P. L., Ussler, W., Steele, J. A., Connon, S. A., Klotz, M. G., and Orphan, V. J.: Abundance

844 and distribution of diverse membrane-bound monooxygenase (Cu-MMO) genes within the Costa Rica

845 oxygen minimum zone, Environ. Microbiol. Reports, 5, 414-423, 2013.

846 Thorpe, S. A., Green, J. A. M., Simpson, J. H., Osborn, T. R., and Nimmo Smith, W. A. M.: Boils and

847 turbulences in a weakly stratified shallow tidal sea, J. Phys. Oceanogr., 38, 1711-1730, 2008.

848 Ursin, E. and Andersen, K. P.: A model of the biological effects of eutrophication in the North Sea,

849 Rapp. P.-v. Reun. Cons. Int. Explor. Mer, 172, 366-377, 1978.

850 Valentine, D. L.: Emerging topics in marine methane biogeochemistry, Annu. Rev. Mar. Sci., 3, 147-

851 171, 2011.

852 Valentine, D. L., Blanton, D. C., Reeburgh, W. S., and Kastner, M.: Water column methane oxidation

853 adjacent to an area of active hydrate dissociation, Eel River Basin, Geochim. Cosmochim. Ac., 65,

854 2633-2640, 2001.

855 Valentine, D. L., Kessler, J. D., Redmond, M. C., Mendes, S. D., Heintz, M. B., Farwell, C., Hu, L.,

856 Kinnaman, F. S., Yvon-Lewis, S., Du, M., Chan, E. W., Tigreros, F. G., and Villanueva, C. J.: Propane

857 respiration jump-starts microbial response to a deep oil spill, Science, 330, 208-211, 2010.

858 Wasmund, K., Kurtboke, D. I., Burns, K. A., and Bourne, D. G.: Microbial diversity in sediments

859 associated with a shallow methane seep in the tropical Timor Sea of Australia reveals a novel aerobic

860 methanotroph diversity, FEMS Microbiol. Ecol., 68, 142–151, 2009.

861 Wenner, P. G., Bell, P. G., van Amerom, F. H. W., Toler, S. K., Edkins, J. E., Hall, M. L., Koehn, K., Short,

862 R. T., and Byrne, R. H.: Environmental chemical mapping using an underwater mass spectrometer,

863 Trac-Trend Anal. Chem., 23, 288-295, 2004.

864 Wiesenburg, D. A. and Guinasso, J. N. L.: Equilibrium solubilities of methane, carbon monoxide, and

865 hydrogen in water and sea water, J. Chem. Eng. Data, 24, 356-360, 1979.

866 Wunsch, C. and Ferrari, R.: Vertical mixing, energy, and the general circulation of the oceans, Annu.

867 Rev. Fluid Mech., 36, 281-314, 2004.

868

869

870 Tables

871 Tab. 1 Classification of partial 16S rRNA gene sequences (Fig. 7) to bacterial taxa performed with the

872 Silva classifier (Pruesse et al., 2012). The confidence value (0–1) for assignment at the level of class

873 and genus is given in parentheses.

No.	Class	Family
1	Alphaproteobacteria (0.4)	*SAR11 clade* (0.2)
2	Cyanobacteria (1)	*Chloroplast* (1)
3	Alphaproteobacteria (1)	*Rhodobacteraceae* (1)
4	Bacteroidetes incertae sedis (0.43)	*Marinifilum* (0.4)
5	Alphaproteobacteria (1)	*Rhodobacteraceae* (1)
6	Alphaproteobacteria (1)	*Rhodobacteraceae* (1)
7	Alphaproteobacteria (1)	*Rhodobacteraceae* (1)
8	Cyanobacteria (1)	*Synechococcus* (1)
9	Cyanobacteria (1)	*Synechococcus* (1)
10	Gammaproteobacteria (1)	*Pseudoalteromonadaceae* (1)
11	Proteobacteria (0.36)	
12	Alphaproteobacteria (1)	*Rhodospirillaceae* (0.8)
13	Alphaproteobacteria (0.91)	*Rhodospirillaceae* (0.7)

874

875

876

877

878

879

880

881

882

883

884

885

886

887

888

889

890

891   Tab. 2 Comparison of highest methane concentrations, methane oxidation rates, and sea-air fluxes from different locations

Location	Methane concentration	MOx-rate	SAF	Reference
	up to nM	nM day^{-1}	nmol m^{-2} s^{-1}	
Seep sites				
central North Sea	1628	0.04-840	0.02-8.3	this study
Coal Oil Point, Santa Barbara Basin	1900	0.02-30	1.8	Mau et al., 2012; Pack et al., 2011
Tommeliten, North Sea	268		10.8*	Schneider von Deimling et al., 2011
west of Prins Karls Forland, Svalbard	524	up to 0.8		Gentz et al., 2013
Eel River Basin	300	0.002-0.8		Valentine et al., 2001
Deepwater Horizon event				
Gulf of Mexico	180000	up to 820		Valentine et al., 2010
Gulf of Mexico	1000000	up to 5900		Crespo-Medina et al., 2014
Overall areas				
Baltic Sea	38		0.008-0.2	Gülzow et al., 2013
Southern Bight of the North Sea	372	0.0002-0.3	0.07-7	Scranton and McShane (1991)
general European shelf estimate	21		0.11-0.24	Bange, 2006
Lakes				
floodplain lake in south-eastern Australia	50000		8.3-2700	Ford et al., 2002
polyhumic lake in southern Finland	150000	30-14400	0.5-695	Kankaala et al., 2007
the subtropical Lake Kinneret in Israel	450000			Eckert and Conrad, 2007
freshwater reservoirs in India	156000			Narvenkar et al., 2013

*direct transport via bubbles

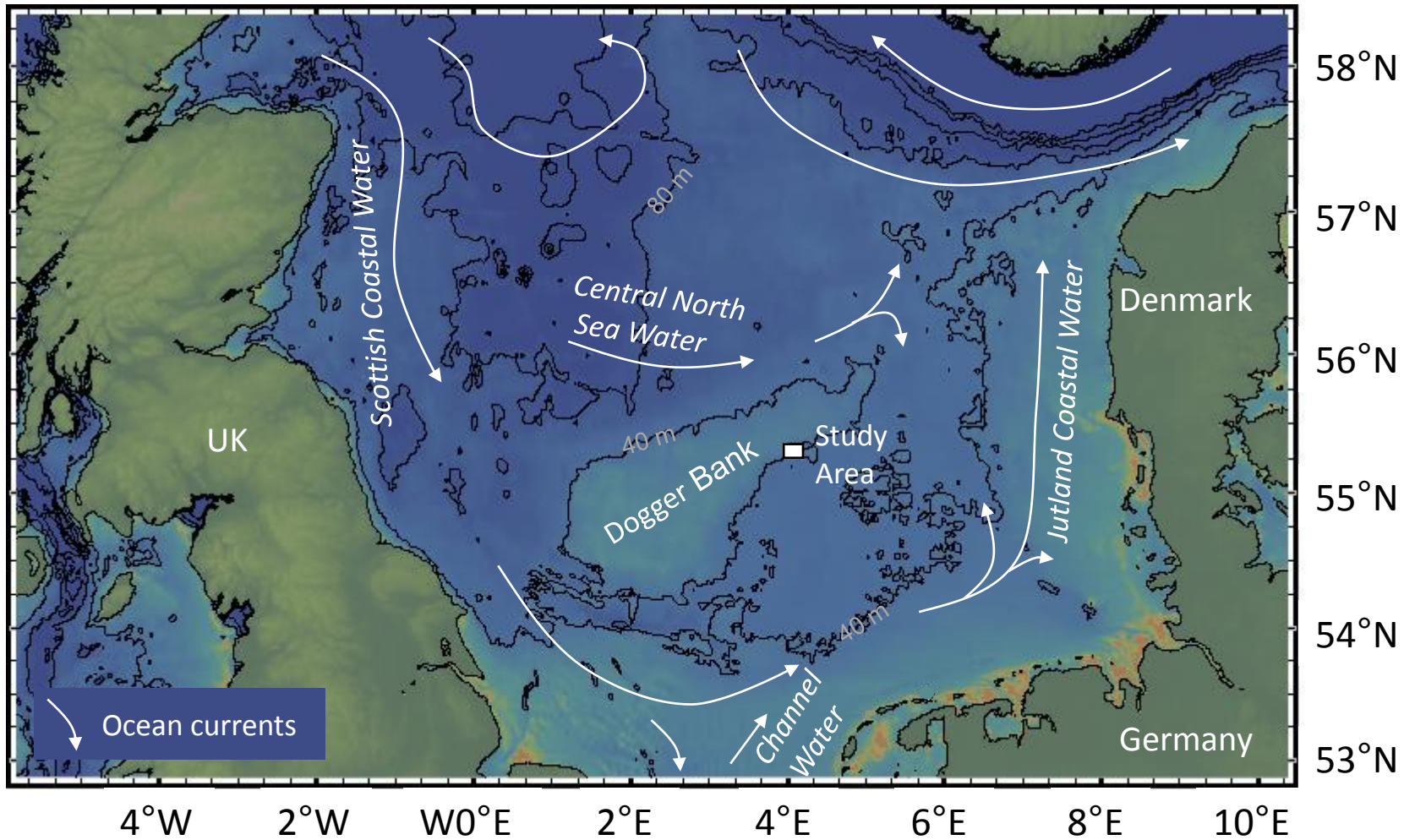892

893

894   Figures

895   Fig. 1: Location of the study area in the central North Sea. The main currents are shown following

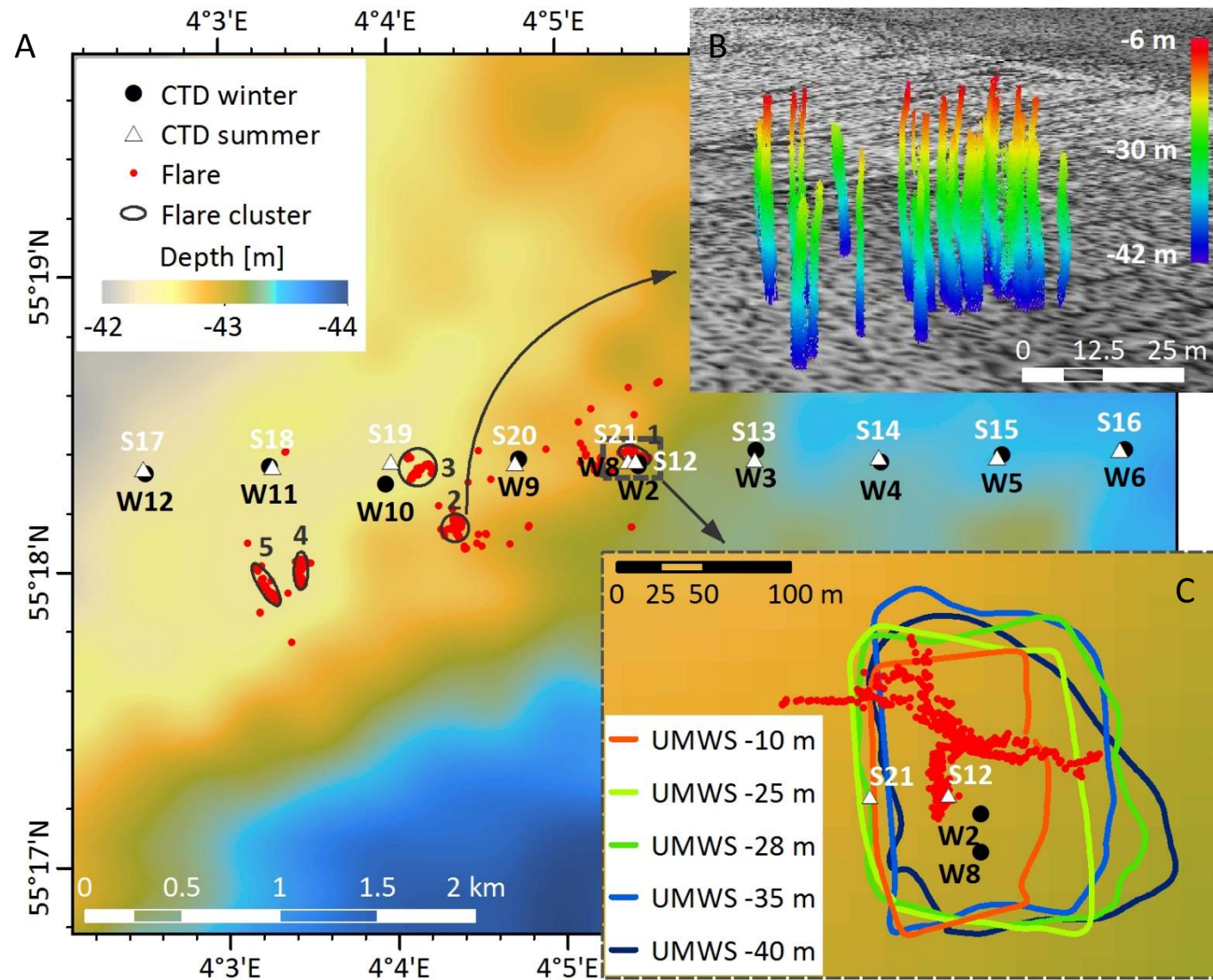896   Howarth (2001). The map was drawn using GeoMapApp with 40 m contours.

897

898   Fig. 2: A) Overview of gas flares mapped in January 2014 and CTD stations sampled in July 2013 (S12-

899   S21) and January 2014 (W2-W12). Flares cluster in 5 distinct areas (cluster 1-5) and reach to 6 m

900   from the sea surface (e.g. cluster 2 (B)), which corresponds to the echosounder's transducer depth.

901   Hence, most likely the gas transport extends to the sea surface. Cluster 1 corresponds to the gas seep

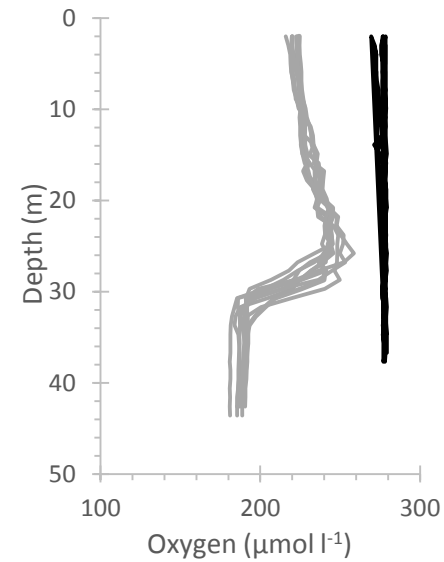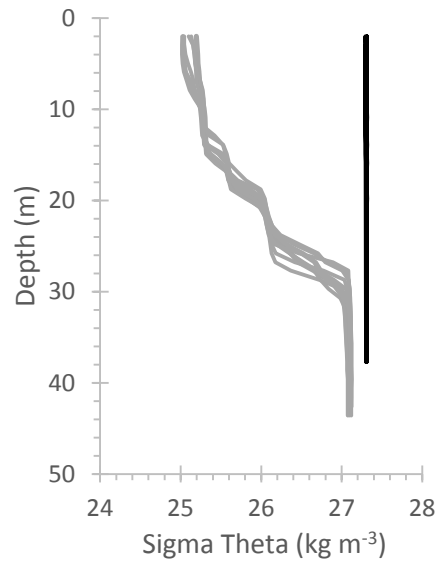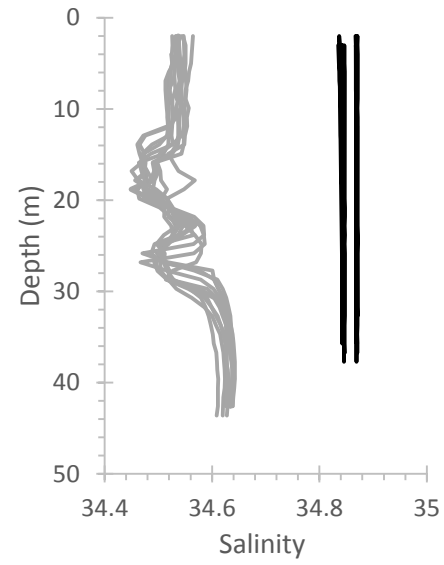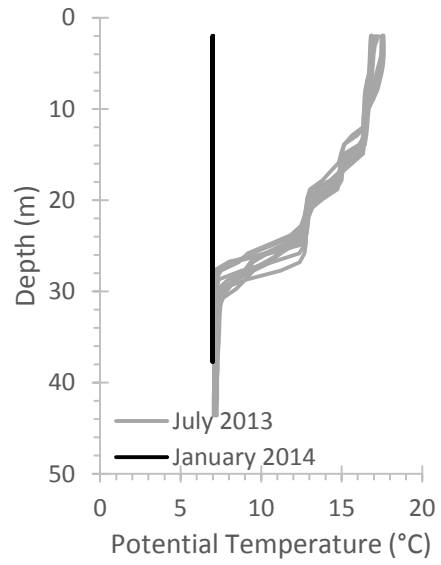902   area investigated by Gentz (2013) (C).

903

904   Fig. 3: Depth profiles of potential temperature, salinity, density (sigma theta), and oxygen for all

905   stations in both summer and winter field programs.
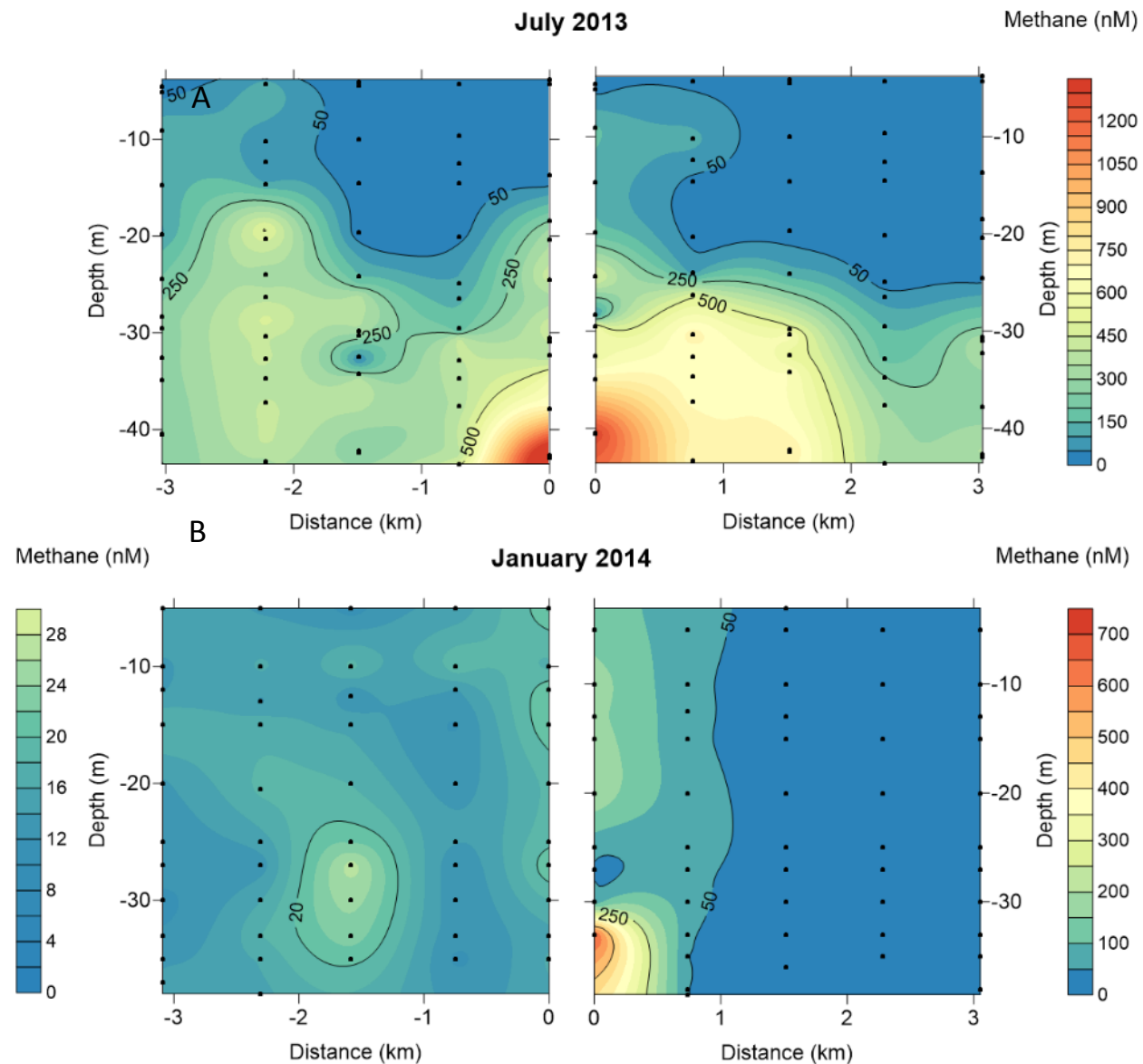
906

907   Fig. 4: A-B Contour plots of the dissolved methane concentrations measured in the water column in

908   July 2013 and January 2014. The 6 km transect was divided into an eastern (positive numbers) and

909   western part (negative numbers) starting from the center station at 0 km. Note the different

910   methane concentration scales, which are necessary to properly display the different concentration

911   ranges. The black dots indicate the sampled water depths.

912

913   Fig. 5: Methane concentrations recorded by UWMS on 21.07.2013 in the vicinity of flare cluster 1

914   (Fig. 2C) at different water depth. The detection limit of the instrument is 16 nM, all measurements

915   below this value are recorded as 0. Apart from temporal and spatial elevations most likely due to

916   bubble streams, the background value is elevated throughout the recording time in 30 and 42 m

917   water depth.

918

919   Fig. 6: Methane oxidation rates versus water depth measured with ^{3}H-methane in July 2013 and in

920   January 2014 (A). B The first order rate constant k' of summer and winter samples indicating the

921   relative activity of the water. C k' versus methane concentration illustrate similar k' values over a

922   wide range of methane concentration. D Methane oxidation rates versus methane concentrations

923   shows for most of the data a first order function: $MOx=0.01[CH_4]^1$ (function with R^2 of 0.92 derived

924   from winter data and with R^2 of 0.85 from summer data).

925

926   Fig. 7: DGGE profile of 16S rRNA gene fragments of samples from different depth and stations in the

927   central North Sea. Numbers on the lines indicate excised and successfully sequenced DGGE bands,

928   whose phylogenetic assignment is listed in Tab. 1.

929

930   Fig. 8: Sketch of transport and loss terms estimated for the study area in nmol m^{-2} s^{-1}.

Fig. 1: Location of the study area in the central North Sea. The main currents are shown following Howarth (2001). The map was drawn using GeoMapApp with 40 m contours.

Fig. 2: A) Overview of gas flares mapped in January 2014 and CTD stations sampled in July 2013 (S12-S21) and January 2014 (W2-W12). Flares cluster in 5 distinct areas (cluster 1-5) and reach to 6 m from the sea surface (e.g. cluster 2 (B)), which corresponds to the echosounder's transducer depth. Hence, most likely the gas transport extends to the sea surface. Cluster 1 corresponds to the gas seep area investigated by Gentz (2013) (C).

Fig. 3: Depth profiles of potential temperature, salinity, density (sigma theta), and oxygen for all stations in both summer and winter field programs.

Fig. 4: A-B Contour plots of the dissolved methane concentrations measured in the water column in July 2013 and January 2014. The 6 km transect was divided into an eastern (positive numbers) and western part (negative numbers) starting from the center station at 0 km. Note the different methane concentration scales, which are necessary to properly display the different concentration ranges. The black dots indicate the sampled water depths.
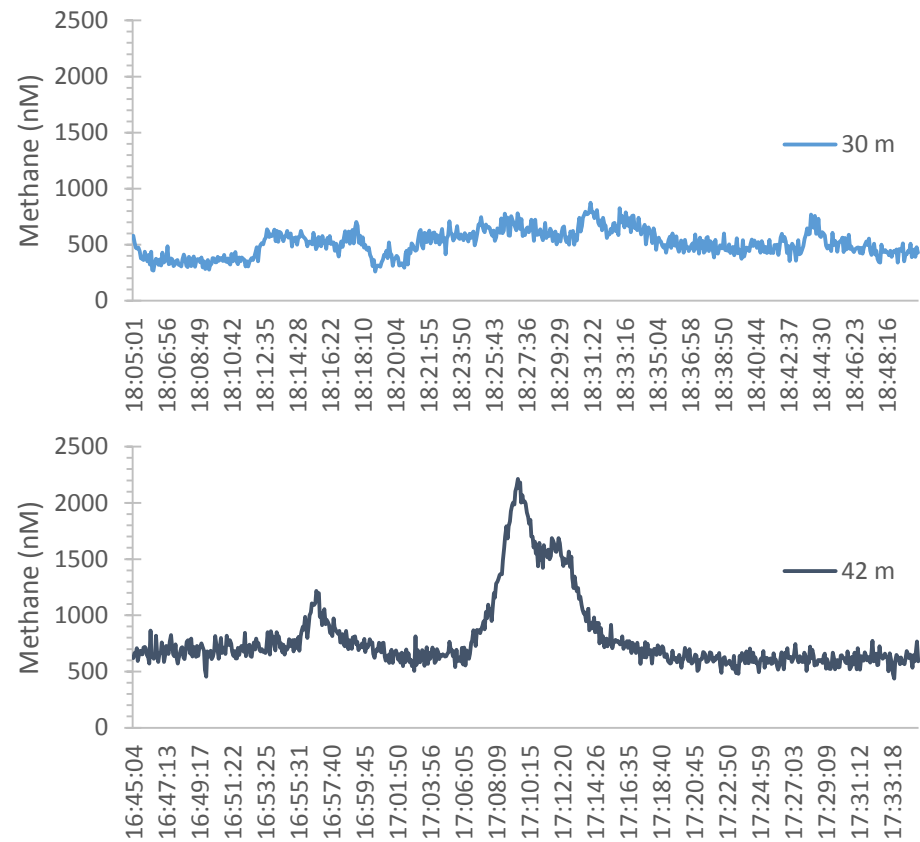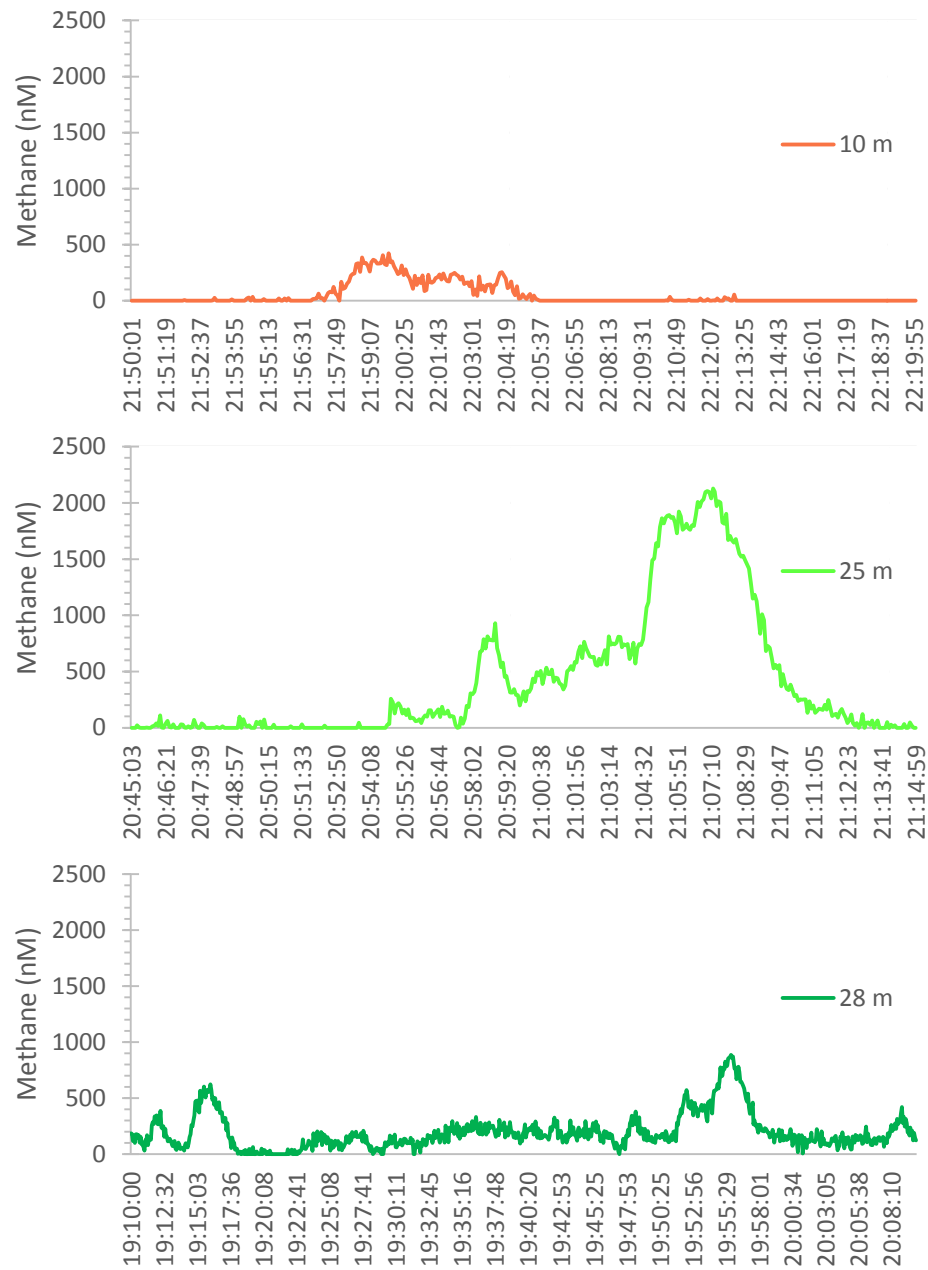
Fig. 5: Methane concentrations recorded by UWMS on 21.07.2013 in the vicinity of flare cluster 1 (Fig. 2C) at different water depth. The detection limit of the instrument is 16 nM, all measurements below this value are recorded as 0. Apart from temporal and spatial elevations most likely due to bubble streams, the background value is elevated throughout the recording time in 30 and 42 m water depth.
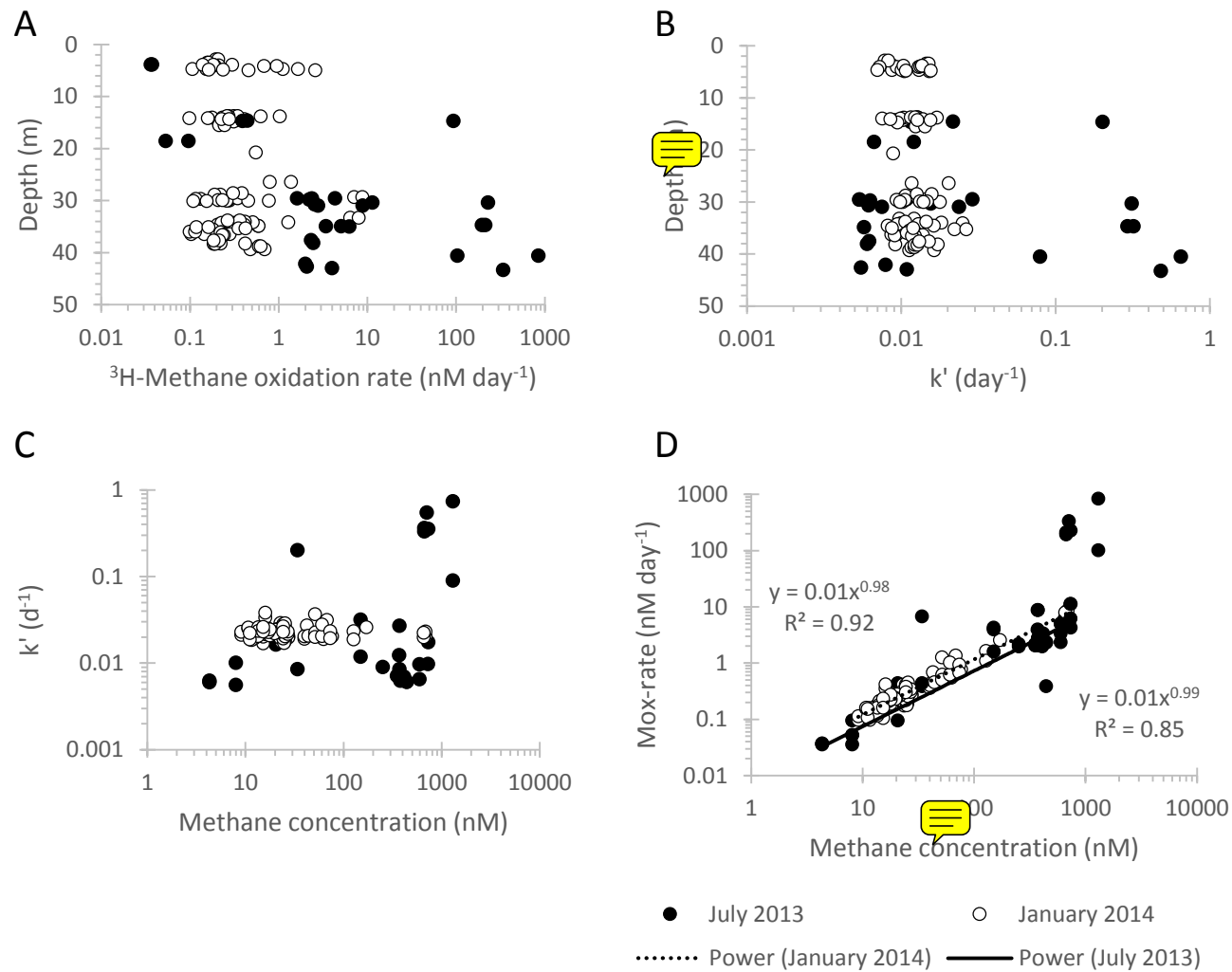
Fig. 6: Methane oxidation rates versus water depth measured with ^{3}H-methane in July 2013 and in January 2014 (A). B The first order rate constant k' of summer and winter samples indicating the relative activity of the water. C k' versus methane concentration illustrate similar k' values over a wide range of methane concentration. D Methane oxidation rates versus methane concentrations shows for most of the data a first order function: $MOx=0.01[CH_4]^1$ (function with R^2 of 0.92 derived from winter data and with R^2 of 0.85 from summer data).
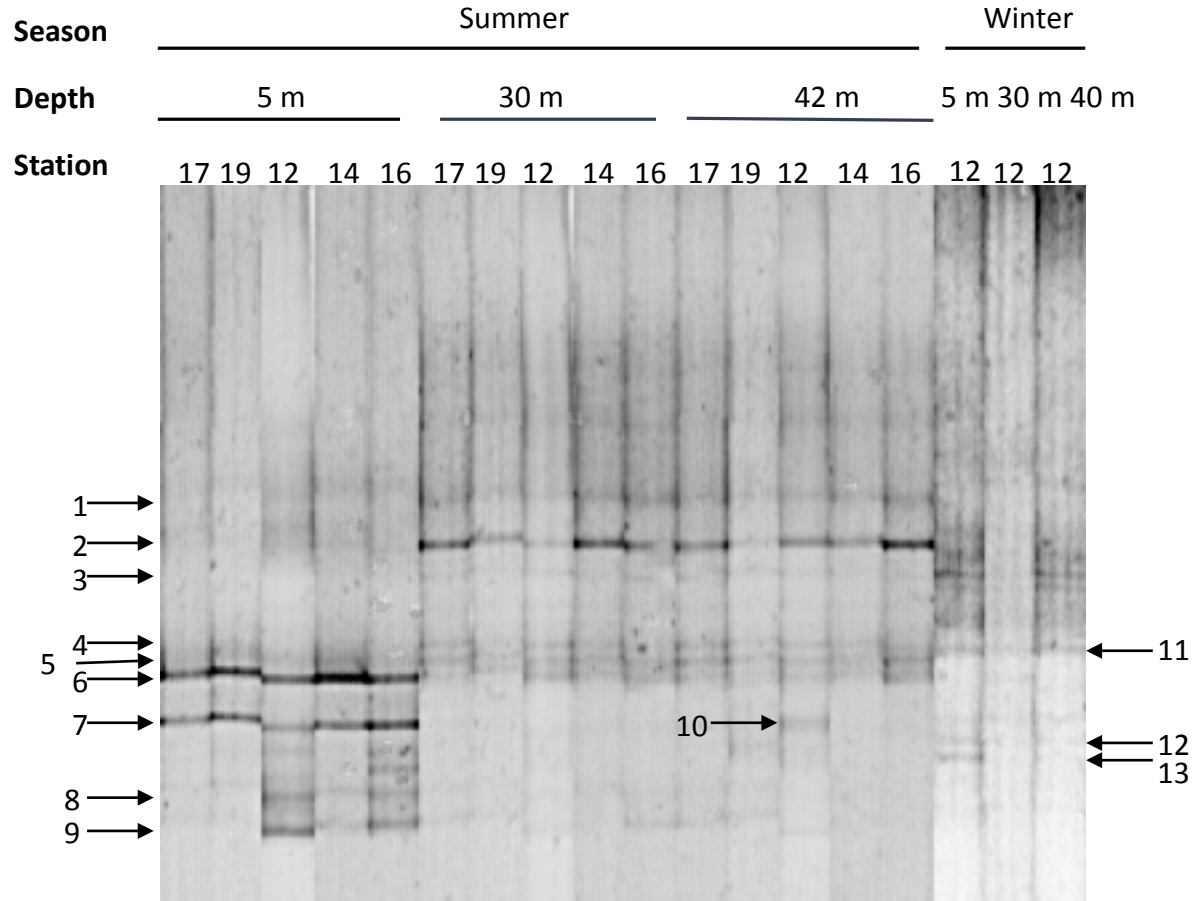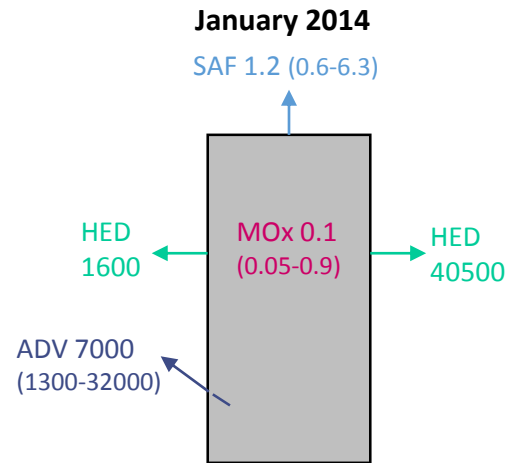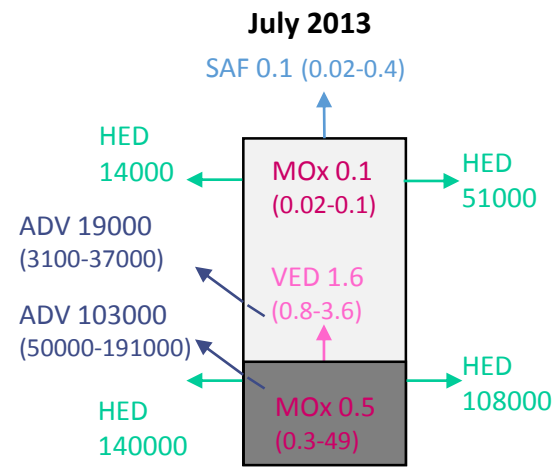
Fig. 7: DGGE profile of 16S rRNA gene fragments of samples from different depth and stations in the central North Sea. Numbers on the lines indicate excised and successfully sequenced DGGE bands, whose phylogenetic assignment is listed in Tab. 1.

Fig. 8: Sketch of transport and loss terms estimated for the study area in nmol m^{-2} s^{-1}.

SAF – Sea Air Flux
MOx – Methane Oxidation rate
VED – Vertical Eddy Diffusion
HED – Horizontal Eddy Diffusion
ADV – Advection
Median of estimates (range of estimates)